Angular distribution control of extreme ultraviolet radiation from laser-produced plasma by manipulating the nanostructure of low-density SnO 2 targets

Applied Physics Letters

Angular distribution control of extreme ultraviolet radiation from laser-produced plasma by manipulating the nanostructure of low-density SnO_2 targets

Cite as: Appl. Phys. Lett. **88**, 094102 (2006); https://doi.org/10.1063/1.2180880
Submitted: 27 June 2005 • Accepted: 17 January 2006 • Published Online: 27 February 2006

Keiji Nagai, QinCui Gu, ZhongZe Gu, et al.

Angular distribution control of extreme ultraviolet radiation from laser-produced plasma by manipulating the nanostructure of low-density SnO_2 targets

Keiji Nagai[a] and QinCui Gu
Institute of Laser Engineering (ILE), Osaka University, 2-6 Yamada-oka, Suita, Osaka 565-0871, Japan

ZhongZe Gu
Biological Science and Medical Engineering, Southeast University Nanjing, Jiangsu 210096, People's Republic of China

Tomoharu Okuno, Shinsuke Fujioka, Hiroaki Nishimura, YeZheng Tao, Yuzuri Yasuda, Mitsuo Nakai, Takayoshi Norimatsu, Yoshinori Shimada, Michiteru Yamaura, Hidetsugu Yoshida, Masahiro Nakatsuka, Noriaki Miyanaga, Katsunobu Nishihara, and Yasukazu Izawa
Institute of Laser Engineering (ILE), Osaka University, 2-6 Yamada-oka, Suita, Osaka 565-0871, Japan

(Received 27 June 2005; accepted 17 January 2006; published online 27 February 2006)

We have found that the divergence of a relatively monochromatic extreme ultraviolet (EUV) emission from a laser-produced plasma can be manipulated by changing the target morphology which is a porous low-density tin oxide (SnO_2) structure. The fundamental light of a Nd-YAG laser was irradiated on the target with laser intensity of $\sim 10^{11}$ W/cm^2 and pulse duration of 10 ns. The nanostructure and density of the targets were tuned by a combination of colloidal polymer template and sol-gel processes [Gu, Nagai, Norimatsu, Fujioka, Nishimura, Nishihara, Miyanaga, and Izawa, Chem. Mater. **17**, 1115 (2005)], which has a merit in large-scale preparation. When the target has an open cell nanostructure, the EUV emission directed predominantly along target normal, while a closed cell target exhibited divergent emission. The angular distribution may be affected by the orientation of the microstructured initial target, and this phenomenon can be applied to wavefront control of EUV emission. © *2006 American Institute of Physics*. [DOI: 10.1063/1.2180880]

Recently, a charming term, "plasma photonics devices," was proposed by Kodama *et al.*[1] Such devices enable us to create a high-energy density state allowed by the delivery of laser energy and shaping of the target. Target fabrication technology has a long history and has further progressed recently through the use of nanotechnology.[2,3] Various target nanomaterials are expected to support plasma photonic devices. Laser-produced plasmas are intensively investigated as one of the most promising extreme ultraviolet (EUV) light sources for the next generation semiconductor lithography industry. The agreed EUV optics in the lithograph system are, at present, Mo/Si multilayer mirrors because of their highest reflectivity for the 13–14 nm wavelength and environment-friendly feature. Sn is a highly efficient material for converting drive laser energy into EUV radiation at 13.5 nm in the 2% bandwidth.[4–10] On the other hand, very strict specifications including high power (115 W), a long lifetime, etc. are demanded for EUV light sources.[11] There is no practical EUV light source system that satisfies the requested specifications for the mass-production of semiconductors due to several technological difficulties.

To control plasma density, low-density and porous materials are often used as laser targets, which have reportedly displayed low-density effects during EUV generation from tin plasma.[8,9,12,13] However, the nano and microstructure effects have not been discussed in laser-produced EUV applications. Some of the authors found a method to prepare 0.5 g/cm^3 SnO_2 targets with a variety of submicroporous structures[14] using a method similar to the so-called inverse opal technique,[15] as follows. A colloidal crystal with monodispersed-1 μm-diameter polystyrene particles was used as the template. A tin solution composed of tin(IV)tetrachloride ($SnCl_4$), ethanol and water was allowed to infiltrate into the voids of the colloidal crystal template and then hydrolyzed to solidify for 4 days. Finally, the composite film was calcined at 400 °C for 5 h to decompose the polystyrene and remove other low-molar-mass chemicals. The resulting tin(IV)dioxide had hierarchical porous nanocrystalline structures with a density of 0.50 ± 0.02 g/cm^3; i.e., there were cellular foams composed of large cells (~ 1 μm), interconnected by windows (200–480 nm), a secondary particle structure (about 10 nm), and nanocrystalline SnO_2 grains (2.4 nm). The window sizes on a submicrometer scale were tuned by the molar ratio of ethanol to tin(IV)tetrachloride. The density of as-prepared porous SnO_2 was maintained constant although the window size and morphology were changed by the content of ethanol. The scanning electron microscopy (SEM) images are shown in Fig. 1.[14] This fabrication procedure has merit in large-scale preparation.

The porous SnO_2 structures were removed from the substrate and a flat face was chosen as the incident direction. EUV plasma generation was carried out using a Nd:YAG laser whose pulse width was 10 ns. The focal spot diameter was fixed at 500 μm. The laser pulse energy was adjusted to attain the laser irradiance ranging from 10^{10} to 10^{11} W/cm^2. The incident angle of the laser beam was normal to the target front face. A target sample area was kept at ~ 4 mm^2.

A monochromatic EUV calorimeter, calibrated using E-mon (Jenoptic inc.), was used to measure the angular distribution of EUV emission from the plasmas. It

[a]Electronic mail: knagai@ile.osaka-u.ac.jp

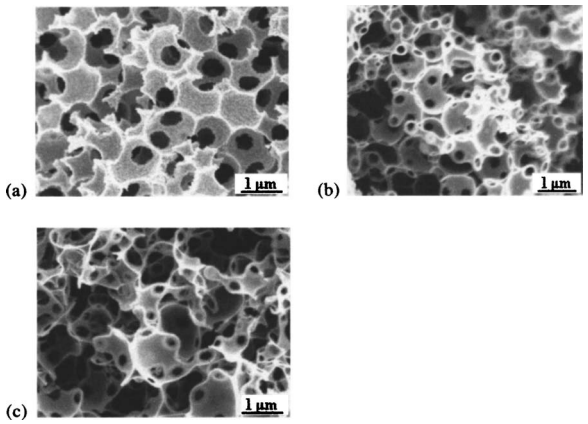

FIG. 1. SEM images of porous SnO_2 prepared with different tin source solutions, where ethanol/$SnCl_4$=2(a), 6(b), and 10(c).

consisted of a 0.2 μm Zr filter overcoated on a 0.1-μm-poly([2,2]paracyclophane) foil, a Mo/Si multilayer mirror of 45° incidence, and an EUV photodiode SXUV-100 from International Radiation Detector. The overall detectable bandwidth was 4% at 13.5 nm. The calorimeter was installed on a semicircular rail and could be moved around the plasma relative to the angle of laser incidence. The signal was recorded with a digital oscilloscope, and was integrated over time to obtain the relative EUV intensity. A grazing incident spectrometer, including a varied-line-space concave grating of 1200 line/mm grooves, was used to observe EUV emission spectra in the range of 6–20 nm. The output spectrum was recorded with a back-illuminated charge coupled device camera and the spectral resolution was 0.06 nm at 13.5 nm.

Figure 2 shows the emission spectra at an incidence of 6×10^{10} W/cm^2. The intensities were normalized by the incident laser power. A peak exists at 13.5 nm which is close to the previously reported wavelength.[7,10]

The angular distribution of radiation reveals information about two-dimensional effect, such as the opacity (reabsorption) effect.[10] The angular distribution of EUV emission $[I(\theta)]$ [sr^{-1}] measured with the monochromatic EUV calorimeter is shown in Fig. 3. These intensities were normalized using the intensity of sample *a* as $I(28)=1$. The data points represent the average of two or three identical shots. The zero-degree of θ represents the direction of target

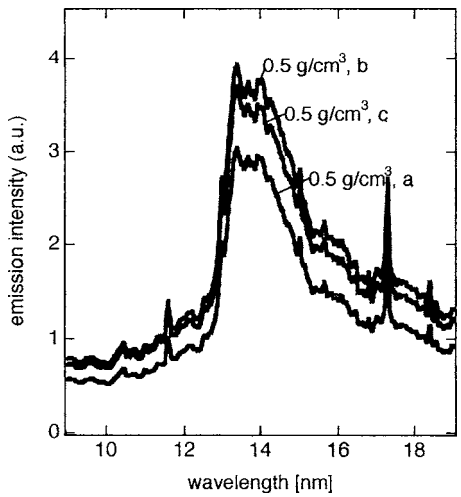

FIG. 2. EUV emission spectra from low-density SnO_2 targets measured by a grazing incident spectrometer. The wavelength was calibrated using line emission at 11.6 nm (O^{5+} 2*s*-4*p*), 13.0 nm (O^{5+} 2*p*-4*d*), 15.0 nm (O^{5+} 2*s*-3*p*), and 17.3 nm (O^{5+} 2*s*-4*p*) (see Ref. 16).

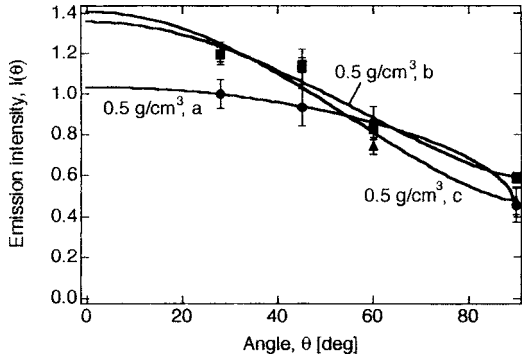

FIG. 3. Angular distribution of EUV emission $[I(\theta)]$ for 0.5 g/cm^2 SnO_2; a, b, and c represent different morphology samples. These intensities were normalized using the intensity of sample a as $I(28)=1$. These data were fitted to Eq. (1) and fitting parameters are shown in Table I

normal. Because of non-negligible emission at 90° ($I(90)$), the angular distribution was analyzed in the following relation:

$$I(\theta) = [I(0) - I(90)]\cos^{\alpha}\theta + I(90), \tag{1}$$

where $I(0)$ is I at $\theta=0$. The parameters in Eq. (1) were obtained by fitting the relation to the data points in Fig. 3 and are summarized in Table I.

Based on these angular distributions, the conversion efficiency (CE) from laser energy to EUV emission can be estimated as follows:

$$\mathrm{CE} = \int_0^{2\pi}\int_0^{\pi/2} [E_{\mathrm{mon45}}/I(45)]I(\theta)d\theta d\Omega, \tag{2}$$

where E_{mon45} means the ratio of EUV 2%-energy per sr in band at 13.5 nm monitored at an angle of 45° to the irradiated laser energy. The CE values were estimated at 2.0, 2.2 and 2.1 for samples a, b, and c, respectively, which were smaller than that for the spherical tin target and 1-ns pulse (3%), due to two dimensional loss and longer laser duration. These CE values remained constant and existed no morphological effect. If the opacity affects the angular distribution, the level of CE should be dependent on the samples.[10] The discrepancy suggests that the opacity effect is not responsible for the EUV divergence.

Another possible reason to explain the variation in divergence is the microscopic random surface orientation of the target. In general, EUV emission distribution is attributable to two-dimensional expansion during laser ablation, i.e., strong for target normal and weak for target lateral directions respectively. For example, an intensity ratio of 30° to that of 75° was almost 2:1 for the tin foil target as reported by Yamaura *et al.*[10] The present porous targets also had a similar tendency, but the ratios were smaller than that of the tin foil as summarized in Table II $[I(30)/I(75)]$. The present targets which were porous materials had various microscopicorientations, and appeared to present a larger surface area normal

TABLE I. Characteristics of low-density SnO_2 and their EUV emissions.

Sample	Ethanol/$SnCl_4$ (mol/mol)	Density (kg/dm^3)	Relative density per bulk SnO_2 (%)	$I(0)$	$I(90)$	α	CE (%)
a	2	0.51	7.3	1.04	0.46	0.53	2.0
b	6	0.52	7.5	1.35	0.59	1.40	2.2
c	10	0.49	7.1	1.46	0.49	1.50	2.1

TABLE II. Target orientation of low-density SnO_2 and their EUV emission orientation.

Sample	S_{nor} (%)	S_{lat} (%)	Relative intensity (calculated) $I_{por}(nor)/I_{por}(lat)$	Relative intensity (experimental) $I(30)/I(75)$
a	26	47	1.0	1.0
b	18	41	1.1	1.3
c	12	49	1.2	1.5

to the laser beam (Fig. 1). In sample a, prepared from low-ethanol content, there is considerable surface area oriented to the target normal, which exhibited a white color area in the SEM images of Fig. 1(a) due to electron shine. Such a face has the capability to radiate for the target lateral. On the other hand, a face-oriented target lateral, which appeared gray in SEM due to a lack of electron shine, has the capability to radiate target normal. The target surfaces were divided into target normal (white) and target lateral (gray) faces as shown in Fig. 4. The other area (black) is holes where the top layer is empty.[14] The areas should be the projection of real three-dimensional target faces, and the projection areas were estimated by counting the pixels in these images and denoting them as S_{nor} and S_{lat} for normal and lateral, respectively. These areas are summarized in Table II, where the order of S_{nor} is as samples a > b > c. The ordering is opposite to the relative emission intensity $[I(30)/I(75)]$ as shown in Table II. In order to interpret them quantitatively, here we assume the intensity ratio of target normal $[I_{tin}(nor)]$ to target lateral $[I_{tin}(lat)]$ to be 2:1, which is based on the intensity ratio of 30° to that of 75° for the tin foil target.[10] From these assumptions, we can roughly estimate the angular distribution for the present data by the following equation as a sum of the product of each of the emission intensity and the projection area, respectively:

$$I_{por}(nor) = I_{tin}(nor)S_{lat} + I_{tin}(lat)S_{nor}, \quad (3)$$

$$I_{por}(lat) = I_{tin}(nor)S_{nor} + I_{tin}(lat)S_{lat}. \quad (4)$$

The relative intensity (calculated) of $I_{por}(nor)/I_{por}(lat)$ is estimated from Eqs. (3) and (4) and shown in Table II. The relative intensity of the experimental value is estimated using the ratio of $I(30)/I(75)$ from Fig. 3. Despite such a rough estimation, there is the same tendency for the ratio to be sample-dependent. The estimated ratios were smaller than the experimental values. A two-dimensional isothermal model on a semi-micrometer scale would be required for further analysis, and the present data would be helpful for two-dimensional simulations.

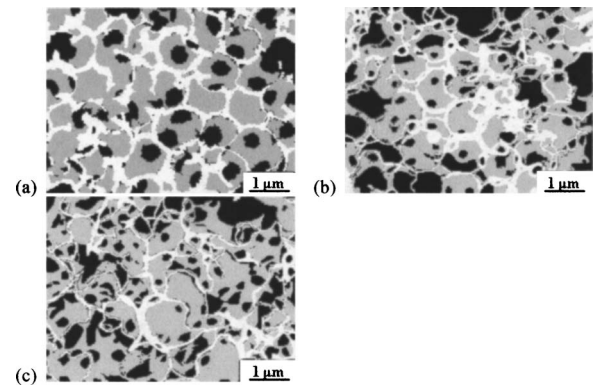

FIG. 4. SEM images of porous SnO_2 prepared with different tin source solutions, where ethanol/$SnCl_4$=2(a), 6(b), and 10(c). The face was mapped for strong shining electron(close to target normal) by white and weak shining electron (close to target lateral) by gray.

Such dependence of EUV emission on the target morphology was found for the first time using the present nanostructure-controlled and low-density target. Because the radiated EUV from the laser plasma is focused by collection mirrors, the beam quality, including the wave front pattern, depends on the angular distribution. This means that the present materials have the capability to control the wave front of EUV emissions.

Considering the practical application for an EUV light source, in addition to the divergence control, the present nanoporous materials have merits of relatively monochromatic emission, a low mass meaning decreased debris and target source. These properties of the present material imply that plasma photonic nanodevices may be used to control EUV light.

A part of this work was performed under the auspices of the Ministry of Education, Culture, Science, and Technology, Japan (MEXT) under the contract subject "Leading project for EUV lithography source development," and was supported by a Grant-in-Aid for Scientific Research in Priority Areas (Fundamental Science and Technology of Photofunctional Interfaces, No. 417 (for two of the authors K. N. and Z. G.) from MEXT.

[1] R. Kodama, Y. Sentoku, Z. L. Chen, G. R. Kumar, S. P. Hatchett, Y. Toyama, T. E. Cowan, R. R. Freeman, J. Fuchs, Y. Izawa, M. H. Key, Y. Kitagawa, K. Kondo, T. Matsuoka, H. Nakamura, M. Nakatsutsumi, P. A. Norreys, T. Norimatsu, R. A. Snavely, R. B. Stephens, M. Tampo, K. A. Tanaka, and T. Yabuuchi, Nature (London) **432**, 1005 (2004).
[2] K. Nagai, T. Norimatsu, Y. Izawa, and T. Yamanaka, *Encyclopedia of Nanoscience and Nanotechnology* Vol. 10, edited by E. H. Nalwa (American Scientific, 2004), p. 407.
[3] K. Nagai, T. Norimatsu, and Y. Izawa, J. Plasma Fusion Res. **80**, 626 (2004).
[4] R. C. Spitzer, T. J. Orzechowski, D. W. Phillion, R. L. Kauffman, and C. Cerjan, J. Appl. Phys. **79**, 2251 (1996).
[5] I.-W. Choi, H. Daido, S. Yamagami, K. Nagai, T. Norimatsu, H. Takabe, M. Suzuki, T. Nakayama, and T. Matsui, J. Opt. Soc. Am. B **17**, 1616 (2000).
[6] P. A. C. Jansson, B. A. M. Hansson, O. Hemberg, M. Otendal, A. Holmberg, J. de Groot, and H. M. Hertz, Appl. Phys. Lett. **84**, 2256 (2004).
[7] Y. Shimada, H. Nishimura, M. Nakai, K. Hashimoto, M. Yamaura, Y. Tao, K. Shigemori, T. Okuno, K. Nishihara, T. Kawamura, A. Sunahara, T. Nishikawa, A. Sasaki, K. Nagai, T. Norimatsu, S. Fujioka, S. Uchida, N. Miyanaga, Y. Izawa, and C. Yamanaka, Appl. Phys. Lett. **86**, 051501 (2005).
[8] Y. Tao, S. Farshad, H. Nishimura, R. Matsui, T. Hibino, T. Okuno, S. Fujioka, K. Nagai, T. Norimatsu, K. Nishihara, N. Miyanaga, Y. Izawa, A. Sunahara, and T. Kawamura, Appl. Phys. Lett. **85**, 1919 (2004).
[9] K. Nagai, H. Nishimura, T. Okuno, T. Hibino, R. Matsui, Y.-Z. Tao, M. Nakai, T. Norimatsu, N. Miyanaga, K. Nishihara, and Y. Izawa, Trans. Mater. Res. Soc. Jpn. **29**, 943 (2004).
[10] M. Yamaura, S. Uchida, A. Sunahara, Y. Shimada, H. Nishimura, S. Fujioka, T. Okuno, K. Hashimoto, K. Nagai, T. Norimatsu, K. Nishihara, N. Miyanaga, Y. Izawa, and C. Yamanaka, Appl. Phys. Lett. **86**, 181107 (2005).
[11] Y. Watanabe, in *Proceedings of the EUV Lithography Source Workshop*, 2005, International SEMATECH, Austin (http://www.sematech.com)
[12] W. L. Perry, R. C. Dye, P. G. Apen, L. Foreman, and E. Peterson, Appl. Phys. Lett. **66**, 314 (1995).
[13] K. Nagai, T. Norimatsu, and Y. Izawa, Fusion Sci. Technol. 45, 79 (2004).
[14] Q.-C. Gu, K. Nagai, T. Norimatsu, S. Fujioka, H. Nishimura, K. Nishihara, N. Miyanaga, and Y. Izawa, Chem. Mater. **17**, 1115 (2005).
[15] Z.-Z. Gu, A. Fujishima, and O. Sato, Appl. Phys. Lett. **85**, 5067 (2004).
[16] C. Keyser, R. Bernath, M. Al-Rabban, and M. Richardson, Jpn. J. Appl. Phys., Part 1 **41**, 4070 (2002).